Spectral element method and the delayed feedback control of chaos

Dennis J. Tweten and Brian P. Mann

Phys. Rev. E **86**, 046214 — Published 31 October 2012

DOI: 10.1103/PhysRevE.86.046214

Spectral element method and the delayed feedback control of chaos

Dennis J. Tweten* and Brian P. Mann†
Mechanical Engineering and Materials Science Department
Duke University
Durham, NC 27708

A new spectral element approach is introduced to determine the Floquet exponents (FEs) of unstable periodic orbits (UPOs) stabilized by extended delayed feedback control (EDFC). The spectral approach does not require solving time dependent eigenproblems that existing methods require. Instead, the spectral approach determines the stability of the delay differential equations of the system by numerical approximation. The method is capable of analyzing systems whose UPOs arise from bifurcations other than period-doubling.

Results are presented for stabilizing UPOs in Duffing systems. The FEs calculated by the spectral approach are compared to published results for two examples. In both cases, the spectral method results agree well with those determined by previous methods. In addition, the spectral method was used to analyze a high dimensional, asymmetrical system with a UPO in chaos arising from tori doubling following a Hopf bifurcation.

PACS numbers: 05.45.-a,82.40.Bj,02.60.-x

I. INTRODUCTION

The method of using delayed feedback to stabilize unstable periodic orbits (UPOs) embedded in a strange attractor was first introduced by Pyragas [1]. In this first implementation of delayed feedback control (DFC), a proportional feedback from a single delay was utilized to stabilize a UPO. This method works well to stabilize period-1 UPOs, but the method often fails to stabilize orbits with longer periods [2]. In addition, DFC has been used for steady-state control in chaotic systems. However, in recent years, alternative approaches such as multiple delay feedback control (MDFC), have been demonstrated to be more effective in stabilizing steady-states [3].

To improve the DFC method, Socolar introduced the extended delayed feedback control (EDFC) method which uses an infinite number of delays while still implemented with a single delay line [4]. The EDFC method has been demonstrated to stabilize UPOs with larger periods [2, 4]. The key to analyzing either method is to determine the Floquet exponents (FEs) of the UPO while under the influence of control. The chief method to calculate the FEs in these first papers was an integration technique by Benettin [2, 5]. The Benettin method is used to identify the largest one or two FEs, but because it relies on increasing the duration of integration to improve accuracy, it is not ideal. In addition, the Benettin method does not provide the imaginary part of the FE.

Advanced techniques using Floquet theory and variational methods have resulted in both approximate [6] and exact [7] methods to determining the FEs of UPOs. These methods greatly improve the ease of determining the FEs by simplifying the delay differential equations (DDEs) into non-autonomous ordinary differential equations (ODEs) [7]. However, the resulting simplification requires one to solve a transcendental eigenproblem. The fact that the variation ODE has non-autonomous coefficients is an additional complication. Pyragas and Just attempted to overcome these complications by assuming the form of the FEs [6, 7]. However, this method is mainly limited to UPOs resulting from period-doubling bifurcations and low dimensional systems [7]. Another recent approach using variational equations was introduced by Tamasevicius [8]. In this method, the time dependent transcendental eigenproblem is reduced to a time independent transcendental eigenproblem by using the time average of the stabilized UPO, but it is limited to weakly nonlinear, symmetrical systems [8].

Rather than simplifying the DDEs to ODES, the DDEs can be solved directly. Analytical solutions to DDEs for weakly nonlinear systems have been developed using the Lambert function [9]. In addition, a number of numerical methods have recently been added to the literature including the semi-discretization [10], collocation [11], and spectral element [12] methods. Each of these numerical techniques has been compared using the delayed Mathieu equation [13] for which analytical solutions have been developed [14].

In this paper, a new method for determining the FEs of UPOs stabilized by EDFC is introduced which is an adaptation of the spectral element method. The spectral element method approximates the infinite dimensional solution to delay differential equations (DDEs) with a finite dimensional solution. The spectral approach does not require any assumptions regarding the form of the FE, determines both the real and imaginary parts of the FEs, and can be applied to highly nonlinear and high-dimensional systems. In addition, the spectral method can be used to analyze systems whose UPOs arise from bifurcations other than period doubling. The spectral

* dennis.tweten@duke.edu
† brian.mann@duke.edu

approach requires numerical integration over the period of the UPO but utilizes quadrature weights which are calculated only once.

This paper is organized in the following way. The first section provides a brief overview of the EDFC method followed by a section describing the implementation of the spectral element method. Simulated examples are then presented using an experimental approach to demonstrate how the EDFC and the spectral element method can be implemented for experiments. Finally, the conclusions are presented.

II. EXTENDED DELAYED FEEDBACK CONTROL

In many chaotic systems, the EDFC method is capable of stabilizing UPOs by applying proportional delayed feedback. The power of the feedback approaches zero once the desired UPO is stabilized [7]. A nonlinear system can be defined by

$$\dot{\mathbf{x}} = \mathbf{f}(\mathbf{x}, t)\,, \tag{1}$$

where $\mathbf{x}$ is a vector of d states and $\mathbf{f}$ is a function of those states and time.

In order to predict whether a particular UPO can be stabilized using the EDFC method, the nonlinear equations must be represented in the variational form

$$\delta\dot{\mathbf{x}} = \mathbf{A}(t)\delta\mathbf{x}\,, \tag{2}$$

$$\mathbf{A}(t) = \mathbf{D}\mathbf{f}(\mathbf{x}_o(t), t)\,, \tag{3}$$

where $\mathbf{x}_o(t)$ is the UPO, $\delta\mathbf{x}$ is the deviation from the UPO, and $\mathbf{A}$ is the $d \times d$ Jacobian. Both the UPO and the Jacobian are periodic with period T that is $\mathbf{x}_0(t) = \mathbf{x}_0(t+T)$ and $\mathbf{A}(t) = \mathbf{A}(t+T)$, respectively. Using Floquet theory, the deviation $\delta\mathbf{x}$ can be represented by

$$\delta\mathbf{x} = \mathbf{u}(t)\mathrm{e}^{\lambda t}\,, \tag{4}$$

where $\mathbf{u}(t) = \mathbf{u}(t+T)$ is a periodic solution and λ is the FE [7]. An UPO has at least one positive FE.

The feedback is applied by an external feedback $\mathbf{F}(t)$ defined by

$$\delta\dot{\mathbf{x}} = \mathbf{A}(t)\delta\mathbf{x} + \mathbf{F}(t)\,, \tag{5}$$

$$\mathbf{F}(t) = \mathbf{K}\left[(1-R)\sum_{r=1}^{\infty} R^{r-1}\mathbf{x}(t-r\tau) - \mathbf{x}(t)\right]\,, \tag{6}$$

where $\mathbf{K}$ is the matrix of proportional gains and R determines the influence of previous delays on the feedback [2]. Note that if $R = 0$, EDFC reduces to DFC in which only a single delay affects the control. The matrix $\mathbf{K}$ can include feedback from and apply control to all the states; however, in many cases control is applied using only one state.

The EDFC method may have difficulty stabilizing UPOs with an odd number of FEs with positive real parts; however, it has been demonstrated that this is not a true limitation of the EDFC method [15, 16]. Adding an additional FE with a positive real part has been shown to overcome this difficulty [8]. Hövel et al. [17] demonstrated limitations of the EDFC method in the presence of latencies in the delay signal. The EDFC method is not strictly limited to stabilizing systems with small Lyapunov exponents, but the range of gains that stabilize systems with large Lyapunov exponents can be very limited [18].

III. SPECTRAL ELEMENT METHOD

The spectral element method is a numerical technique of approximating the infinite dimensional solution of DDEs by a finite dimensional system [12]. The method is based on the method of weighted residuals and is a convenient way of determining the stability of delay systems.

A general DDE for a linearized or variational system with multiple delays is given by

$$\dot{\mathbf{x}}(t) = \mathbf{A}(t)\mathbf{x}(t) + \sum_{r=1}^{n_\tau} \mathbf{B}_r(t)\mathbf{x}(t-\tau_r), \tag{7}$$

where $\mathbf{x}(t)$ is a column vector of d states, $\mathbf{A}(t)$ is the $d \times d$ Jacobian, τ_r is the duration of the r^{th} delay, the delay matrices $\mathbf{B}_r(t)$ are the dependencies of the states on the delayed states $\mathbf{x}(t-\tau_r)$, n_τ is the number of delays, and τ_{n_τ} is the duration of the longest delay. In general, the Jacobian $\mathbf{A}(t)$ will be a function of the UPO of interest which makes the DDE non-autonomous. In addition, the Jacobian and the delay matrices $\mathbf{B}_r$ are periodic so that $\mathbf{A}(t) = \mathbf{A}(t+T)$ and $\mathbf{B}_r(t) = \mathbf{B}_r(t+T)$. When control is implemented for more than one state or for cross coupling, the matrix $\mathbf{K}$ will have more than one non-zero entry. In either of these cases, the Jacobian will include gain terms in more than one element, and the delay matrices are created by premultipling a matrix of the delay terms on the diagonal with the matrix $\mathbf{K}$. The second example in Section IV demonstrates this more general case.

The stability of a UPO can be determined from the eigenvalues of the monodromy operator of the system. The monodromy operator maps the delay states from the segment $[-\tau_{n_\tau}, 0]$ to the current period $[0, T]$, and the operator's eigenvalues are the Floquet multipliers of the UPO. However, the monodromy operator acts on an infinite dimensional state space so it is impractical to deal with the operator directly [12]. The spectral element method approximates the infinite dimensional monodromy operator with a finite dimensional monodromy matrix $\mathbf{U}$ [12]. The monodromy matrix maps a finite number of states by

$$\mathbf{x}_m = \mathbf{U}\mathbf{x}_{m-1}\,, \tag{8}$$

where $\mathbf{U}$ maps the states $\mathbf{x}_{m-1}$ from the time segment $[-\tau_{n_\tau}, 0]$ onto the states $\mathbf{x}_m$ which includes the period

$[0, T]$ [12]. The spectral approach requires that the equations of the system be arranged in a variational form so that each state is the deviation from the UPO, and the monodromy matrix then becomes a function of the UPO. The eigenvalues of the monodromy matrix in this form $\mathbf{U}(t, \mathbf{x}_0(t))$ are the Floquet multipliers of the UPO which includes both real and imaginary terms. The Floquet multipliers are related to the FEs by

$$\mu = \exp(\lambda T)\,, \tag{9}$$

where λ is the FE and $\mathbf{x}_0(t)$ is the UPO.

The first step in applying the spectral element method to EDFC is to approximate the solution using polynomial trial functions ϕ_i given by

$$\mathbf{x}_j(t) = \sum_{i=1}^{n+1} \mathbf{x}_{j,i}\,\phi_i(\eta), \tag{10a}$$

$$\mathbf{x}_j(t - r\tau) = \sum_{i=1}^{n+1} \mathbf{x}_{j,i-rn}\,\phi_i(\eta)\,, \tag{10b}$$

where ϕ_i is the trial function, η is the local time normalized from 0 to 1 for the element j, r is a particular delay, and τ is the delay equal to the period of the UPO [19]. The vector $\mathbf{x}_{j,i}(t)$ is the value of the states of the j^{th} element at the i^{th} node [12]. A total of $n+1$ interpolation nodes are used for each element. In general, the spectral element method can be implemented with an arbitrary delay, but for forced systems the delays will be multiples of the forcing period. The solution can also be broken into multiple elements of arbitrary duration. However, while the notation for multiple elements is included in this paper, the examples will be implemented with one element.

We have selected the Legendre-Gauss-Lobatto (LGL) points for the interpolation nodes. The LGL nodes are computed from the roots of the polynomial $(1-u^2)L'_n(u)$ where $L_n(u)$ is the n^{th} order Legendre function, $L'_n(u)$ is the first derivative of $L_n(u)$ with respect to u, and u is on the segment $[-1, 1]$ [12]. The LGL nodes must therefore be shifted to be on the segment $[0, 1]$ in order to be compatible with Eq. (10). The trial functions ϕ_i can be found using the barycentric Lagrange formula

$$\phi_i(t) = \frac{\frac{\rho_i}{t-t_i}}{\sum_{j=1}^{n+1} \frac{\rho_j}{t-t_j}}\,, \tag{11}$$

and the barycentric weights ρ_i given by

$$\rho_i = \frac{1}{\prod_{k=1,k\neq i}^{n+1} (t_i - t_k)},\ k = 1, 2, \ldots, n+1\,, \tag{12}$$

where t_i and t_k represent time at the i^{th} and k^{th} nodes, respectively [20]. The barycentric Lagrange interpolation used in Eq. (11) improves the numerical stability of larger meshes when compared to the more commonly used Lagrangian interpolation [21]. The trial functions have the useful property

$$\phi_i(t_k) = \delta_{i,k}\,,\ t_k \in \{t_i\}_{i=1}^{n+1}\,, \tag{13}$$

which means the combined term $\mathbf{x}_{j,i}\,\phi_i(\eta)$ is the value of the states at each node. The derivatives of the trial functions can also be calculated using the barycentric formula as

$$\phi'_i(t_k) = \begin{cases} \frac{\rho_i/\rho_k}{t_i - t_k}, & i \neq k \\ \sum\limits_{i=0, i\neq k}^{n+1} \frac{-\rho_i/\rho_k}{t_i - t_k}, & i = k. \end{cases} \tag{14}$$

For a matrix $\mathbf{D}$ with elements $D_{ki} = \phi'_i(t_k)$, the derivative of a vector of states $\mathbf{z}$ on a mesh of LGL nodes is given by $\mathbf{z}\,' = \mathbf{D}\mathbf{z}$ [12].

A nonlinear DDE in variational form can now be approximated with polynomial test functions by substituting Eqs. (10)(13)(14) into Eq. (7). The method of weighted residuals is then used to minimize the error of the polynomial approximation by setting the approximate DDE to zero and integrating over the duration of each element [12]. The method of weighted residuals requires multiplication of the approximate solution by a test function for which we have selected Legendre polynomials. The resulting integration is given by

$$\int_0^1 \left(\frac{1}{t_j} \mathbf{x}_{j,i}\,\phi'_i(\eta) - \mathbf{A}(t_\eta)\mathbf{x}_{j,i}\,\phi_i(\eta) - \sum_{r=1}^{n_\tau} \mathbf{B}_r(t_\eta)\mathbf{x}_{j,i-rn}\,\phi_i(\eta) \right) \psi_p(\eta)\,\mathrm{d}\eta = 0, \tag{15}$$

where $\psi_p(\eta)$ is the p^{th} Legendre polynomial, η is the normalized time in each element, and $t_\eta = (\eta + j - 1)t_j$.

The speed of the integration is increased by using by using quadrature weights rather than symbolic integration. The numerical integration of a function by quadrature weights is given by

$$\int_0^1 f(\eta)\,\mathrm{d}\eta \approx \sum_{k=1}^{n+1} w_k f(\eta_k), \tag{16}$$

where w_k is the quadrature weight and η_k is the localized time at the node k. For a grid of LGL points, the quadrature weights [22] are given by

$$w_k = \begin{cases} \frac{2}{n(n+1)} & k = 1, n+1 \\ \frac{2}{n(n+1)(L_n(\eta_k))^2}, & \text{otherwise}\,. \end{cases} \tag{17}$$

Quadrature weights are calculated in advanced and reused for each integration.

Implementing the method of weighted residuals with quadrature rates results in Eq. (18) on the next page. The matrices $\mathbf{N}$ and $\mathbf{P}$ are sub-matrices of matrices $\mathbf{H}$

$$\begin{bmatrix} \mathbf{I} & \mathbf{0} & \dots & \mathbf{0} \\ \mathbf{N}^1_{j,i} & \mathbf{N}^1_{j,i+1} & \dots & \mathbf{N}^1_{j,i+n} \\ \mathbf{N}^2_{j,i} & \mathbf{N}^2_{j,i+1} & \dots & \mathbf{N}^2_{j,i+n} \\ \vdots & \vdots & \ddots & \vdots \\ \mathbf{N}^n_{j,i} & \mathbf{N}^n_{j,i+1} & \dots & \mathbf{N}^n_{j,i+n} \end{bmatrix} \begin{bmatrix} \mathbf{x}_{j,i} \\ \mathbf{x}_{j,i+1} \\ \vdots \\ \mathbf{x}_{j,i+n} \end{bmatrix} = \begin{bmatrix} \mathbf{0} & \dots & \mathbf{0} & \mathbf{0} & \dots & \mathbf{0} & \mathbf{I} \\ \mathbf{P}^1_{j,i-rn} & \dots & \mathbf{P}^1_{j,i-rn+n} & \mathbf{P}^1_{j,i-n(r-1)+1} & \dots & \mathbf{P}^1_{j,i-1} & \mathbf{P}^1_{j,i} \\ \mathbf{P}^2_{j,i-rn} & \dots & \mathbf{P}^2_{j,i-rn+n} & \mathbf{P}^2_{j,i-n(r-1)+1} & \dots & \mathbf{P}^2_{j,i-1} & \mathbf{P}^2_{j,i} \\ \vdots & \ddots & \vdots & \vdots & \ddots & \vdots & \vdots \\ \mathbf{P}^n_{j,i-rn} & \dots & \mathbf{P}^n_{j,i-rn+n} & \mathbf{P}^n_{j,i-n(r-1)+1} & \dots & \mathbf{P}^n_{j,i-1} & \mathbf{P}^n_{j,i} \end{bmatrix} \begin{bmatrix} \mathbf{x}_{j,i-kn} \\ \vdots \\ \mathbf{x}_{j,i-rn+n} \\ \mathbf{x}_{j,i-n(r-1)+1} \\ \vdots \\ \mathbf{x}_{j,i-1} \\ \mathbf{x}_{j,i} \end{bmatrix} \tag{18}$$

and $\mathbf{G}$, respectively. The sub-matrix $\mathbf{I}$ is the $d \times d$ identity matrix. These elements are defined by

$$\mathbf{N}^p_{j,i} = \sum_{k=1}^{n+1} \left(\frac{1}{t_j} \mathbf{I} \phi_i'(\eta_k) \psi_p(\eta_k) w_k \right) - \mathbf{A}(t_\eta) \psi_p(\eta_i) w_i \tag{19a}$$

$$\mathbf{P}^p_{j,i-rn} = \mathbf{B}_r(t_\eta) \psi_p(\eta_i) w_i \tag{19b}$$

where all elements are $d \times d$ matrices [12]. The indexes j refers to the j^{th} element, i to the i^{th} node, and p to the p^{th} order Legendre polynomial. The $\mathbf{N}$ matrices are defined by the upper half of Eq. (15) on the period $[0, T]$, and the $\mathbf{P}$ matrices are defined by the lower half of Eq. (15) on the delay periods. Equation (18) can be simplified to

$$\mathbf{H}\mathbf{x}_m = \mathbf{G}\mathbf{x}_{m-1}\,, \tag{20}$$

where $\mathbf{x}_m$ includes only the states in the period $[0, T]$ and $\mathbf{G}$ and $\mathbf{H}$ are of unequal size if more than one delay is included.

The final step to determine the FE of the DDEs in Eq. (7) is to construct the monodromy matrix $\mathbf{U}$ from Eq. (8). Using the matrices $\mathbf{G}$ and $\mathbf{H}$ and mapping identical states results in

$$\mathbf{U}(\mathbf{x}_0(t), t) = \begin{bmatrix} \mathbf{0}_{D_3 \times d \cdot E \cdot n} & \mathbf{I}_{D_3 \times D_3} & \mathbf{0}_{D_3 \times d} \\ & \mathbf{H}^{-1}\mathbf{G} & \end{bmatrix} \tag{21}$$

where $D_1 = d(1 + n \cdot E)$, $D_2 = d(n_\tau \cdot E \cdot n + 1)$, $D_3 = D_2 - D_1$, and the size of $\mathbf{H}^{-1}\mathbf{G}$ is $D_1 \times D_2$. The vector $\mathbf{x}_m$ includes states in the period $[0, T]$ and enough delay states to be of equal length as $\mathbf{x}_{m-1}$. The added delay states in $\mathbf{x}_m$ is required to make the monodromy matrix square. The additional states are mapped directly to the identical states in $\mathbf{x}_{m-1}$ through the identity matrix $\mathbf{I}_{D_3 \times D_3}$.

IV. EXAMPLES

The analog implementation of the EDFC method incorporates an infinite number of delays for values of $R > 0$ using a single delay line. However, when applying the spectral approach to approximate a system with EDFC, only a finite number of delays is practical. The limitation of a finite number of delays is not intractable since the influence of longer delays decrease exponentially.

Keeping with an experimental approach, we chose the number of grid points $n + 1$ and number of delays n_τ for each example using the following strategy. Starting with the case $R = 0$ where only one delay is required, we increased the number of grid points until the plot of the maximal FE versus the gain no longer changed with additional grid points. At the maximal number of grid points, the approximation was considered converged. This number of grids points for plots were used for cases where $R > 0$. For each value of R, we increased the number of delays n_τ until the maximal Floquet exponent curve no longer changed with additional delays.

An experimental approach was also selected for extracting the UPOs from the simulated results. The equations were simulated for 5×10^5 units of time and sampled 100 times per forcing period. Potential UPOs were identified by using a procedure similar to the one proposed by Lathrop and Kostelich [23]. The absolute value of the difference of the states between the beginning and end of an orbit period where compared to a percentage of the maximum variation in each state. These comparisons were carried out for each data point for a subset of the total simulation. In cases where the difference of each state was less than 5% of the total range for each state, the time span was identified as a potential UPO. Identified UPOs were grouped by shape and period. The UPOs in each group were approximated by a Fourier series and the coefficients of the series were averaged. The resulting averaged Fourier series provided good approximations of the UPOs in each example.

It should be noted that the spectral element approach for EDFC is not limited to the Duffing equation. We chose systems based on the Duffing equation because they are well known and are common in physical systems. The equations for a Duffing system under EDFC control is given by

$$\dot{x} = y \tag{22a}$$

$$\dot{y} = -\mu y + \beta_1 x - \beta_3 x^3 + a\cos(\Omega t) + F(x, y, t) \tag{22b}$$

where μ is the damping; β_1 and β_3 are the restoring force

coefficients; a is the forcing amplitude; and Ω is the forcing frequency.

The first example is a Duffing system used by Pyragas [2] to demonstrate the capability of EDFC to stabilize orbits that could not be stabilized by DFC. The control input for this example is

$$F(x,y,t) = K\left[(1-R)\sum_{r=1}^{\infty} R^{r-1}y(t-r\tau) - y(t)\right], \tag{23}$$

where the control is based solely on the state y. The Jacobian $\mathbf{A}$ and the delay matrices $\mathbf{B}_r$ are given by

$$\mathbf{A} = \begin{bmatrix} 0 & 1 \\ \beta_1 - 3\beta_3 x_0^2(t) & -\mu - K \end{bmatrix}, \tag{24a}$$

$$\mathbf{B}_r = \begin{bmatrix} 0 & 0 \\ 0 & KR^{r-1}(1-R) \end{bmatrix}, \tag{24b}$$

where $x_0(t)$ is the position of the desired UPO and r is the number of periods T in each delay. In Figs. 1a and 1b, the maximal Floquet exponent is plotted versus the gain K with $R = 0$, 0.2, 0.4, 0.6, and 0.8 for a period-1 and period-3 UPO, respectively. A total number of 55 nodes were used for the period-1 UPO and 60 nodes for the period-3 UPO. The UPO is plotted as an insert in the upper right corner of each figure with x as the independent variable and y as the dependent variable. Both figures show excellent agreement with Pyragas [2]. The control parameters that stabilized both UPOs are listed in Table I. The stable gains were taken from Fig. 1 and rounded to the nearest hundredth. Note that for the period-1 example, the maximum gain of $K = 2$ is listed in Table I to correspond to the largest gain considered, but the maximum stable gain is larger for values of $R = 0.2$ and greater.

TABLE I. Control parameters which stabilized the period-1 and period-3 UPOs in Example 1. Stable gains were taken from Fig. 1 and rounded to the nearest hundredth. Note that for period-1, the maximum gain of $K = 2$ is listed to correspond to the largest gain considered, but the maximum stable gain is larger for values of $R = 0.2$ and greater.

Period-1					
R	0.0	0.2	0.4	0.6	0.8
K	0.27-1.99	0.32-2.00	0.37-2.00	0.43-2.00	0.48-2.00
Period-3					
R	0.0	0.2	0.4	0.6	0.8
K				0.38-0.43	0.43-0.56

The second example is taken from Tamasevicius [8] for which the period-1 UPO has an odd number of Floquet multipliers greater than unity. Tamasevicius introduced a clever method for adding an unstable mode by adding an additional state to the system [8]. The updated state

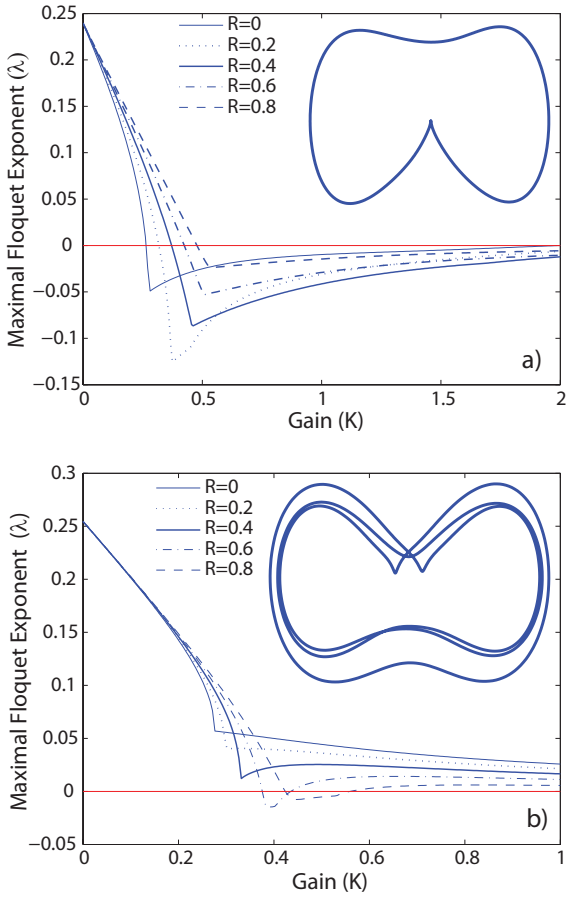

FIG. 1. (Color online) Example 1: Maximal Floquet exponent λ of the stabilized period-1 orbit in figure (a) and the period-3 orbit in figure (b) versus the gain K. The parameters for the system are $\beta_1 = 1$, $\beta_3 = 1$, $\mu = 0.02$, $a = 2.5$, and $\Omega = 1$.

equations are given by

$$\dot{x} = y\,, \tag{25a}$$

$$\dot{y} = -\mu y + \beta_1 x - \beta_3 x^3 + a\cos(\Omega t) - KW + F(x,y,t)\,, \tag{25b}$$

$$\dot{W} = \lambda_c W - bF(x,y,t)\,, \tag{25c}$$

where W is the added state, b is an additional control gain, and λ_c is the positive, real FE due to the added state [8]. The addition of an unstable Floquet exponent is one strategy to stabilize the UPO using EDFC. The control input $F(x,y,t)$ is given by

$$F(x,y,t) = K\left[(1-R)\sum_{r=1}^{\infty} R^{r-1}x(t-r\tau) - x(t)\right], \tag{26}$$

where the control is influenced by the delays of state x. The implementation of the matrix $\mathbf{K}$ is given by

$$\mathbf{K} = \begin{bmatrix} 0 & 0 & 0 \\ K & 0 & 0 \\ -Kb & 0 & 0 \end{bmatrix}, \tag{27}$$

and the Jacobian $\mathbf{A}$ and the delay matrices $\mathbf{B}_r$ are given by

$$\mathbf{A} = \begin{bmatrix} 0 & 1 & 0 \\ \beta_1 - 3\beta_3 x_0^2(t) & -\mu & -K \\ 0 & 0 & \lambda_c \end{bmatrix} - \mathbf{K}\,, \tag{28a}$$

$$\mathbf{B}_r = \mathbf{K} \begin{bmatrix} R^{r-1}(1-R) & 0 & 0 \\ 0 & R^{r-1}(1-R) & 0 \\ 0 & 0 & R^{r-1}(1-R) \end{bmatrix}. \tag{28b}$$

Note that in this case of multiple gains and cross-coupling, the delay matrix $\mathbf{B}_r$ is created by premultipling the delay states with the matrix $\mathbf{K}$. Also note that in this example the gain K is used both as a coupling parameter in the Jacobian $\mathbf{A}$ and as a gain in the delay matrix $\mathbf{B}_r$. In Fig. 2 the three largest Floquet exponents are plotted versus the gain K with $R = 0.9$ for a period-1 UPO. A total number of 30 nodes were used in the spectral approach analysis. In this case the period-1 UPO is elliptical and is not shown. There is excellent agreement between the spectral element approach and the averaged UPO approach used by Tamasevicius [8].

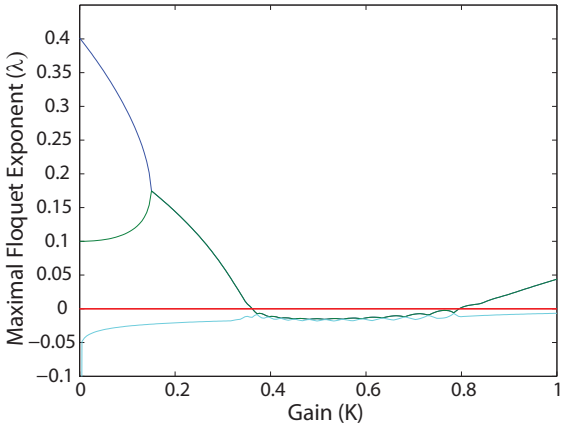

FIG. 2. (Color online) Example 2: Maximal Floquet exponent λ of the stabilized period-1 orbit of the Duffing oscillator versus the gain K. The parameters for the system are $\beta_1 = 0.3$, $\beta_3 = 0.3$, $\mu = 0.3$, $a = 0.27$, $\Omega = 1$, $\lambda_c = 0.1$, $b = 0.2$, and $R = 0.9$.

The third and last example was selected to demonstrate the capability of the spectral approach to find the FEs of a UPOs for which previous methods are not fully capable of analyzing. For instance, the UPO in this example occurs in chaos arising from tori doubling which occurs after a Hopf bifurcation. Since a Hopf bifurcation does not tend to occur in a simple Duffing system [24], we selected a system with two identical, coupled Duffing oscillators studied by Kenfack [25] which also makes it a higher order system. The UPO, as shown in Fig. 3, is also non-symmetrical.

The equations for the identical coupled oscillators have the same form used in Eq. (22) with the first oscillator having the states x_1 and y_1 and the second oscillator having the states x_2 and y_2. The only difference is a linear coupling element C between states x_1 and x_2. The implementation of the Jacobian $\mathbf{A}$ and the delay matrix $\mathbf{B}_r$ are given by

$$\mathbf{A} = \begin{bmatrix} 0 & 1 & 0 & 0 \\ \alpha_1 & -\mu - K & C & 0 \\ 0 & 0 & 0 & 1 \\ C & \alpha_2 & -\mu & 0 \end{bmatrix} \tag{29a}$$

$$\mathbf{B}_r = \begin{bmatrix} 0 & 0 & 0 & 0 \\ 0 & KR^{r-1}(1-R) & 0 & 0 \\ 0 & 0 & 0 & 0 \\ 0 & 0 & 0 & 0 \end{bmatrix}, \tag{29b}$$

where $\alpha_1 = \beta_1 - 3\beta_3 x_{10}^2(t) - C$, $\alpha_2 = \beta_1 - 3\beta_3 x_{20}^2(t) - C$, x_{10} is the path of the UPO for state x_1, and x_{20} is the path of the UPO for state x_2. Forcing and control are applied to the state y_1.

The stabilization of the period-1 UPO is show in Fig. 3 with the UPO for the states x_1 and y_1 plotted as an insert in the lower right corner. For this example the UPO was estimated from the system under EDFC. The maximal FE is plotted versus the gain K with $R = 0$, 0.2, 0.4, 0.6, and 0.8. A total number of 38 nodes were used in the spectral approach analysis. No changes to the spectral approach were required to accommodate the additional states or even the asymmetry. The control parameters that stabilized the period-1 UPO are listed in Table II. Note that the maximum gain of $K = 2$ is listed in Table II to correspond to the largest gain considered, but the maximum stable gain is larger for each value of R. The stable gains were taken from Fig. 3 and rounded to the nearest hundredth.

In addition to the spectral approach, the Benettin method was used to analyze the case with $R = 0.6$. Results for gains stepped by 0.1 were plotted as stars in Fig 3. A total number of 200 to 400 delay states were required for the Benettin method to approach convergence at each gain, and the equations had to be integrated for at least 250 periods. Figure 3 shows good agreement between the spectral approach and the Benettin method.

Figure 4 provides a root locus plot of the period-1 orbit for the system in Eq. (29). The crosses indicate select FEs with gains of $K = 0$, and the unstable FEs have the value of $\lambda = 0.041 \pm i0.32$. The maximum gain used in the plot is $K = 500$, and select FEs determined from this gain are indicated by large dots.

A continuous simulation of the coupled Duffing system was performed with a value of $R = 0.6$. In the simulation, the gain K was discretely stepped by 0.01 from 0 to 2 with 2000 units of simulation time between each step. The results in Fig. 5 show excellent agreement with the spectral element method. The spectral element method indicated a gain of about $K = 0.14$ was required for control. The simulation required a gain of $K = 0.151$ for control which was determined using a second, extended simulation with a single gain.

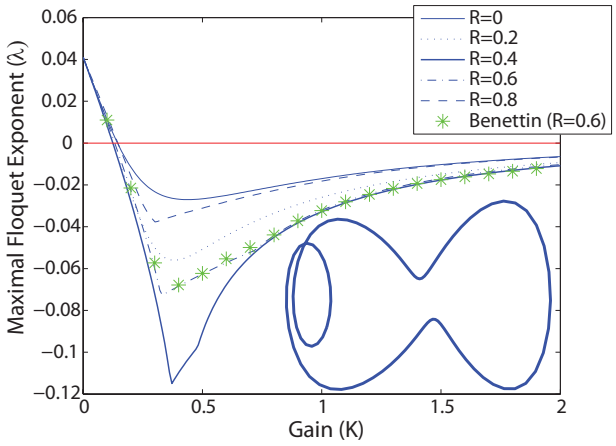

FIG. 3. (Color online) Example 3: Maximal Floquet exponent λ of the stabilized period-1 orbit of the Coupled Duffing oscillators versus the gain K. The coupled oscillators have the identical parameters of $\beta_1 = 1$, $\beta_3 = 1$, $\mu = 0.1$, $C = 5$, $a = 15$, and $\Omega = 1.12$.

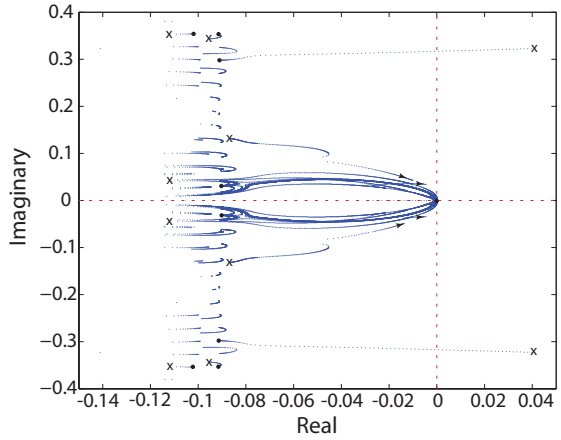

FIG. 4. (Color online) Example 3: Root Locus plot for the case $R = 0.6$ and period-1 orbit. Crosses show the location of roots for gains of $K = 0$, and large dots indicate roots for $K = 500$. The initially unstable FEs ($K = 0$) begin at $\Re(\lambda) = 0.041$ and $\Im(\lambda) = \pm 0.32$.

TABLE II. Control parameters which stabilized the period-1 UPO in Example 3. Stable gains were taken from Fig. 3 and rounded to the nearest hundredth. Note that the maximum gain of $K = 2$ is listed to correspond to the largest gain considered, but the maximum stable gain is larger for each value of R.

R	0.0	0.2	0.4	0.6	0.8
K	0.15-2.00	0.13-2.00	0.13-2.00	0.14-2.00	0.15-2.00

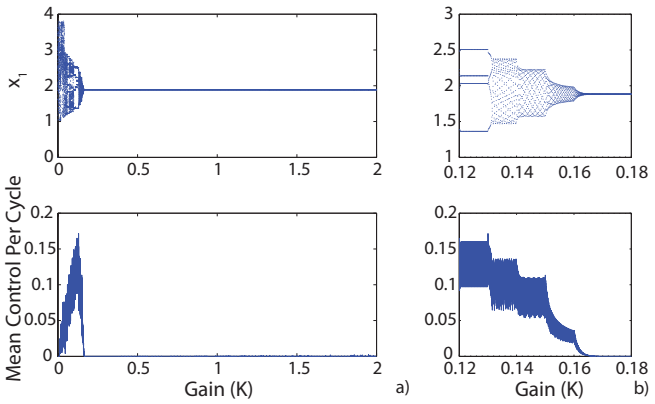

FIG. 5. (Color online) Example 3: Time response of the coupled Duffing oscillators versus the gain K for $R = 0.6$ and period-1 orbit. Figure (a) shows all values of K stepped by 0.01 from 0 to 2, while figure (b) shows the critical region between 0.12 and 0.18. The upper graphs show the response of the first oscillator sampled ten times per forcing period. The lower graphs show the absolute value of the control averaged over each period.

V. CONCLUSIONS

The spectral element approach was introduced which is a new method to determine the FEs of UPOs stabilized by EDFC. The spectral approach approximates the infinite dimensional monodromy operator with a finite dimensional monodromy matrix. The eigenvalues of the monodromy matrix are the Floquet multipliers from which the FEs can be determined. The advantage of the spectral approach is that DDEs can be solved directly without the complications that occur when the DDEs are simplified into ODEs. Unlike the existing analytical method used by Pyragas [7], the spectral approach does not require any assumptions regarding the form of the FE and can be applied to highly nonlinear and high dimensional systems. The spectral approach also provides both the real and imaginary parts of the FE unlike the existing Benettin numerical method. Most importantly, the spectral element method can be used to analyze systems whose UPOs arise from bifurcations other than period-doubling.

The spectral approach was applied to Duffing system examples including UPOs stabilized by both DFC and EDFC. Also, an example of an UPO with an odd number of unstable FEs was stabilized after adding an unstable FE. The FEs calculated by the spectral approach were compared to results published using previously established methods. In both cases, the spectral method results agreed well with the previously published results. Finally, the spectral element method was used to analyze a higher dimensional, asymmetrical system with a UPO in chaos arising from tori doubling. The resulting analysis agreed well with the numerical simulation.

ACKNOWLEDGMENTS

The authors would like to acknowledge financial support from the U.S. National Science Foundation through grant no. CMMI-0900266.

[1] K. Pyragas, Phys. Lett. A **170**, 421 (1992).
[2] K. Pyragas, Phys. Lett. A **206**, 323 (1995).
[3] E. Schöll and H. G. Schuster, *Handbook of Chaos Control*, 2nd ed. (Wiley-VCH, 2008).
[4] J. Socolar, D. Sukow, and D. Gauthier, Phys. Rev. E **50**, 3245 (1994).
[5] G. Benettin, C. Froeschle, and J. P. Scheidecker, Phys. Rev. A **19**, 2454 (1979).
[6] W. Just, T. Bernard, M. Ostheimer, E. Reibold, and H. Benner, Phys. Rev. Lett. **78**, 203 (1997).
[7] K. Pyragas, Phil. Trans. R. Soc. A **364**, 2309 (2006).
[8] A. Tamaševičius, G. Mykolaitis, V. Pyragas, and K. Pyragas, Phys. Rev. E **76**, 026203 (2007).
[9] A. Amann, E. Schöll, and W. Just, Physica A **373**, 191 (2007).
[10] T. Insperger, G. Stépán, and J. Turi, J. Sound Vib. **313**, 334 (2008).
[11] E. Butcher and O. Bobrenkov, Commun. Nonlinear Sci. Numer. Simul. **16**, 1541 (2011).
[12] F. Khasawneh and B. P. Mann, Int. J. Numer. Methods Eng. **87**, 566 (2011).
[13] D. Tweten, G. Lipp, F. Khasawneh, and B. Mann, J. Sound Vib. **331**, 4057 (2012).
[14] T. Insperger and G. Stepan, Proc. R. Soc. Lond. A **458**, 1989 (2002).
[15] B. Fielder, V. Flunkert, M. Georgi, P. Hövel, and E. Schöll, Phys. Rev. Lett. **98**, 114101 (2007).
[16] W. Just, B. Fiedler, M. Georgi, V. Flunkert, P. Hövel, and E. Schöll, Phys. Rev. E **76**, 026210 (2007).
[17] P. Hövel and J. Socolar, Phys. Rev. E **68**, 036206 (2003).
[18] W. Just, E. Reibold, H. Benner, K. Kacperski, P. Fronczak, and J. Holyst, Phys. Lett. A **254**, 158 (1999).
[19] F. Khasawneh and B. Mann, Commun. Nonlinear Sci. Numer. Simul. (2012), submitted.
[20] N. Higham, IMA J. Numer. Anal. **24**, 547 (2004).
[21] J. Berrut and L. N. Trefethen, SIAM Review **46**, 501 (2004).
[22] S. Parter, J. Sci. Comput. **14**, 347 (1999).
[23] D. P. Lathrop and E. J. Kostelich, Phys. Rev. A **40**, 4028 (1989).
[24] J. Kozlowski, U. Parlitz, and W. Lauterborn, Phys. Rev. E **51**, 1861 (1995).
[25] A. Kenfack, Chaos, Solitons Fractals **15**, 205 (2003).